

# Ferroelectric-like behaviour of the SmCP phase in liquid crystalline compounds with asymmetrical bent-core molecules

V. Novotná,<sup>\*a</sup> M. Kašpar,<sup>a</sup> V. Hamplová,<sup>a</sup> M. Glogarová,<sup>a</sup> L. Lejček,<sup>a</sup> J. Kroupa<sup>a</sup> and D. Pocięcha<sup>b</sup>

Received 23rd January 2006, Accepted 2nd March 2006

First published as an Advance Article on the web 22nd March 2006

DOI: 10.1039/b601084a

A new series of asymmetrical bent-shaped mesogens has been synthesised and their mesomorphic properties studied. All compounds exhibit the B<sub>2</sub> (SmCP) phase. For some compounds we found a very low coercive field for switching to the saturated ferroelectric state and only one peak in the switching current. Due to the lack of SHG signal in the zero field state and the behaviour of the relaxation mode we cannot unambiguously assign ferroelectric or antiferroelectric character to the B<sub>2</sub> phase observed. The observation of planar samples revealed a striped texture. Large optically active domains appear on very slow cooling, which are attributed to a non-homogeneous (twisted) in-plane structure imposed by surfaces. The twisted domains are suppressed under a critical electric field. A simple model of such a structure and its behavior in the electric field is proposed. The low temperature phase detected on further cooling is attributed to a crystalline-like smectic phase.

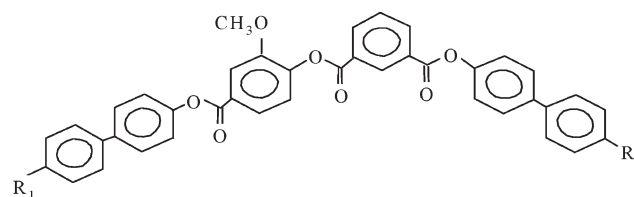
## Introduction

The discovery of polar switching in banana-like mesogens in 1996 opened a new direction in the field of liquid crystals.<sup>1</sup> The spontaneous polarization in such materials results from the in-layer close packing of bent-shaped molecules. The polar switching occurs in the B<sub>2</sub> phase, the phase with liquid like smectic layers and molecules tilted with respect to the layer normal. The combination of molecular tilt and layer polarization makes each smectic layer structurally chiral.<sup>2</sup> In ref. 2 four phase structures of the B<sub>2</sub> phase were distinguished using the nomenclature SmC<sub>S,A</sub>P<sub>F,A</sub>, by which the synclinc (S) or anticlinc (A) molecular tilt correlation and the ferroelectric (F) or antiferroelectric (A) polar correlation between adjacent layers are described. The chirality of subsequent layers can alternate producing an overall racemic state, or can be the same in neighbouring layers forming a homochiral phase. The antiferroelectric synclinc (SmC<sub>S</sub>P<sub>A</sub>) and ferroelectric anticlinc (SmC<sub>A</sub>P<sub>F</sub>) structures are racemic, while the antiferroelectric anticlinc (SmC<sub>A</sub>P<sub>A</sub>) and ferroelectric synclinc (SmC<sub>S</sub>P<sub>F</sub>) structures are chiral.<sup>2</sup> Most of the B<sub>2</sub> phases known so far have an antiferroelectric ground (field free) state<sup>2–8</sup> and both types of antiferroelectric domains, SmC<sub>S</sub>P<sub>A</sub> and SmC<sub>A</sub>P<sub>A</sub>, have been observed. An attempt to obtain a ferroelectric B<sub>2</sub> phase was made by Walba *et al.*<sup>3</sup> introducing a chiral chain, the same as that in the antiferroelectric compound MHPOBC with rod-like molecules. The compound exhibited the stable ferroelectric phase SmC<sub>A</sub>P<sub>F</sub>. Further detailed studies<sup>9</sup> of textures and SHG analysis clarified the ferroelectricity of the observed B<sub>2</sub> phase in another compound with a chiral moiety or with a chiral admixture.<sup>10</sup> Nevertheless, the mechanism of emergence of ferro- or antiferroelectricity is not yet clear, but

we can speculate about interactions between terminal chains of adjacent layers.

In spite of intensive research of symmetrical bent-shaped mesogens,<sup>3–11</sup> questions concerning the relationship between molecular structure and mesomorphic properties are still open. We have synthesized several series of non-chiral mesogens composed of symmetric bent-shaped molecules with thermally stable ester linkages and a core laterally substituted by a methoxy group.<sup>7,11</sup> The first studied symmetrical mesogens exhibited the B<sub>2</sub>–B<sub>7</sub> phase sequence on cooling from the isotropic phase.<sup>11</sup> Recently, attempts to diminish the symmetry of molecules have appeared<sup>12–19</sup> with the expectation that a new shape of molecules would provide novel features of mesophases. Following this idea we changed the character of the end groups asymmetrically using the double bond at the end of one of the aliphatic chains. This modification resulted in a shift of phase transition temperatures, the phase sequence remaining conserved.<sup>20</sup> Herein, instead of a symmetrical core with seven phenyl rings<sup>7,11,20</sup> we have used an asymmetrical bent core with six phenyl rings, laterally substituted by a methoxy group (Scheme 1).

We have studied the mesomorphic behaviour of a new series with asymmetrical bent cores and the physical properties are presented. Texture observation, switching studies in an electric field, dielectric spectroscopy, X-ray analysis and SHG



**Scheme 1** General formula of studied compounds. Alkyl and alkoxy chains R<sub>1</sub>, R<sub>2</sub> are –OC<sub>n</sub>H<sub>2n+1</sub>, –C<sub>n</sub>H<sub>2n+1</sub> and/or –OC<sub>9</sub>H<sub>18</sub>CH=CH<sub>2</sub>.

<sup>a</sup>Institute of Physics, Academy of Sciences of the Czech Republic, Na Slovance 2, 182 21 Prague 8, Czech Republic. E-mail: novotna@fzu.cz

<sup>b</sup>Laboratory of Dielectrics and Magnetism, Chemistry Department, Warsaw University, Al. Zwirki i Wigury 101, 02-089 Warsaw, Poland

measurements have been performed. A model describing the texture behaviour in an electric field has been proposed.

## Experimental

### Synthesis

The general synthesis route is outlined in Scheme 2. First, mesogenic phenols  $M_1$  and  $M_2$  were prepared, which will form the arms of the banana molecules. These phenols contain alkyl or alkoxy chains, or an alkoxy chain with a terminal double bond.  $M_1$  phenols, where  $R_1 = -OC_nH_{2n+1}$ , were prepared from 4'-alkoxybiphenyl-4-ol and 3-methoxy-(4-methoxycarbonyloxy)benzoyl chloride in a mixture of pyridine and chloroform as has been described in detail in ref. 7. Phenols  $M_1$  and  $M_2$ , with  $-C_nH_{2n+1}$  chains, were prepared by Friedel-Crafts acylation of 4-acetyloxybiphenyl and subsequent reduction of the keto group in a zinc/hydrochloric acid mixture as described in ref. 21. Phenols  $M_1$  and  $M_2$  with  $-OC_9H_{18}CH=CH_2$  chains were prepared by the same route as in Ref. 20 using 1-bromo-10-undecene as a starting material.

Mesogenic acids **1** were obtained by esterification of mesogenic phenols  $M_1$  (20 mmol) by 15 g of isophthaloyl dichloride in dichloromethane/pyridine solution. The reaction mixture was refluxed for 4 hours and left to stand at room temperature overnight. Then 50 ml of dioxane and 10 ml of water were added and the mixture was stirred for one hour at room temperature. The mixture was washed with dilute HCl and the excess of unreacted isophthalic acid was separated by filtration. The filtrate was washed with water and the solvent was evaporated. The solid residue crystallized from glacial acetic acid contained a small amount of symmetrical product **2**. Further purification was carried out by recrystallization from ethanol in which symmetrical product **2** is more soluble than acid **1**.

$^1\text{H-NMR}$  **1**,  $R_1 = OC_{11}H_{23}$ : 8.97 s (1H, HAr between  $-\text{COO}$  in isoph. acid); 8.4 dd (2H, HAr *ortho* to  $-\text{COO}$  in isoph. acid); 7.95 d (1H, HAr *para* to  $-\text{OCH}_3$ ); 7.4–7.7 m (1H, HAr *meta* to  $-\text{COO}$  in isoph. acid + 4H HAr *ortho* to  $-\text{Ar}$ ); 7.3 m (3H, HAr *ortho* to  $-\text{OCO}$ ); 6.97 d (2H, HAr *ortho* to  $-\text{OCH}_2$ ); 4.0 t (2H,  $\text{CH}_2\text{OAr}$ ); 3.95 s (3H,  $-\text{OCH}_3$ ); 1.8 quint (2H,  $\text{CH}_2\text{CH}_2\text{OAr}$ ); 1.2–1.6 m (16H,  $\text{CH}_2$ ); 0.9 t (3H,  $\text{CH}_3$ ).

Mesogenic acids **1** were converted into the corresponding acyl chlorides **3** by reflux of dry acids with the excess of the oxalyl chloride overnight. Then the oxalyl chloride was distilled off *in vacuo*, the residue was dissolved in

dichloromethane, filtered and the solution was used for esterification of mesogenic phenol  $M_1$  using standard reaction conditions.

$^1\text{H-NMR}$  **3**,  $R_1 = OC_{11}H_{23}$ : 8.98 s (1H, HAr between  $-\text{COO}$  and  $\text{COCl}$ ); 8.56 d (1H, HAr *ortho* to  $-\text{COCl}$ ); 8.40 d (1H, HAr *ortho* to  $-\text{COO}$ ); 7.95 d (1H, HAr *para* to  $-\text{OCH}_3$ ); 7.7 t (1H, HAr *meta* to  $-\text{COCl}$ ); 7.5 and 7.6 dd (4H, HAr *ortho* to  $-\text{Ar}$ ); 7.3 m (3H, HAr *ortho* to  $-\text{OCO}$ ); 7.0 d (2H, HAr *ortho* to  $-\text{OCH}_2$ ); 4.0 t (2H,  $\text{CH}_2\text{OAr}$ ); 3.95 s (3H,  $-\text{OCH}_3$ ); 1.8 quint (2H,  $\text{CH}_2\text{CH}_2\text{OAr}$ ); 1.2–1.6 m (16H,  $\text{CH}_2$ ); 0.9 t (3H,  $\text{CH}_3$ ).

Final products were prepared by esterification in a pyridine/dichloromethane mixture using standard reaction conditions. The crude product was crystallized from a toluene/acetone mixture, purified by column chromatography on silica gel using a mixture of dichloromethane and acetone (99.5 : 0.5) as eluent and crystallized twice from acetone. The structures of all final products **4a–i** were confirmed by  $^1\text{H-NMR}$  (200 MHz,  $\text{CDCl}_3$ , Varian, Gemini 2000). The chemical purity of the compounds was checked by high pressure liquid chromatography (HPLC), which was carried out with an Ecom HPLC chromatograph using a silica gel column (Separon 7  $\mu\text{m}$ ,  $3 \times 150$ , Tessek) with a mixture of 99.9% of toluene and 0.1% of methanol as eluent, and detection of the eluting products by a UV-VIS detector ( $\lambda = 290$  nm). The chemical purity was found to be more than 99.9% under these conditions.

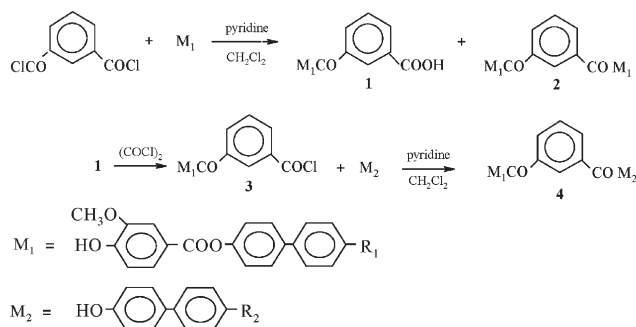
$^1\text{H-NMR}$  **4d** ( $R_1 = -C_{11}H_{21}$ ,  $R_2 = -OC_{11}H_{23}$ ): 9.05 s (1H, HAr between  $-\text{COO}$  in isoph. acid); 8.5d (2H, *ortho* to  $-\text{COO}$  in isoph. acid); 7.95 dd (1H, *para* to  $-\text{OCH}_3$ ); 7.82 s (1H, *ortho* to  $-\text{OCH}_3$ ); 7.78 t (1H, *meta* to  $-\text{COO}$  in isoph. acid); 7.4–7.6 m (8H, *ortho* to Ar); 7.25 m (7H, *ortho* to  $-\text{OCO}$ , *ortho* to  $-\text{R}$ ); 7.0 d (2H, HAr *ortho* to  $-\text{OR}$ ); 4.0 t (2H,  $\text{CH}_2\text{OAr}$ ); 3.95 s (3H,  $-\text{OCH}_3$ ); 2.65 t (2H,  $-\text{CH}_2\text{Ar}$ ); 1.2–1.8 m (36H,  $\text{CH}_2$ ); 0.95 m (6H,  $\text{CH}_3$ ).

$^1\text{H-NMR}$  **4h** ( $R_1 = -OC_{10}H_{21}$ ,  $R_2 = -OC_9H_{18}CH=CH_2$ ): 9.0 s (1H, HAr between  $-\text{COO}$  in isoph. acid); 8.4–8.6 dd (2H, *ortho* to  $-\text{COO}$  in isoph. acid); 7.95 dd (1H, *para* to  $-\text{OCH}_3$ ); 7.82 s (1H, *ortho* to  $-\text{OCH}_3$ ); 7.78 t (1H, *meta* to  $-\text{COO}$  in isoph. acid); 7.4–7.6 m (8H, HAr *ortho* to  $-\text{Ar}$ ); 7.3 m (5H, *ortho* to  $-\text{OCO}$ ); 7.0 d (4H, *ortho* to  $-\text{OR}$ ); 5.82 m (1H,  $\text{CH}_2=\text{CH}-$ ); 5.0 m (2H,  $\text{CH}_2=\text{CH}-$ ); 4.0 t (4H,  $\text{CH}_2\text{OAr}$ ); 3.95 s (3H,  $-\text{OCH}_3$ ); 2.1 q (2H,  $\text{CH}_2=\text{CH}-\text{CH}_2$ ); 1.8 quint (4H,  $\text{CH}_2\text{CH}_2\text{OAr}$ ); 1.2–1.6 m (28H,  $\text{CH}_2$ ); 0.9 t (3H,  $\text{CH}_3$ ).

### Experimental techniques

All synthesised materials were studied using DSC (Perkin-Elmer Pyris Diamond). The compounds with a mass of about 5 mg were hermetically closed in aluminium pans. The samples were placed in a nitrogen atmosphere and cooling and heating rates of  $5 \text{ K min}^{-1}$  were applied.

Observation of textures in liquid crystalline phases represents an essential tool for phase identification. A Nikon Eclipse E-600 polarizing microscope was used. The temperature was changed and stabilized with an accuracy of  $\pm 0.1^\circ \text{C}$  in the hot stage (Linkam). The samples were filled in the isotropic phase into cells composed of glass plates provided with ITO electrodes. The sample thickness was  $3.5 \mu\text{m}$ . Free-standing films (FSF) were prepared by spreading a melted compound over the hole in the metal slab.



Scheme 2 Synthesis route.

Switching studies were performed using the driving voltage from a Phillips generator PM 5191 accompanied by a linear amplifier, which allowed a maximum amplitude of  $\pm 120$  V to be reached. A LeCroy 9304 memory oscilloscope provided information about the switching current profile vs. time.

For dielectric measurements, we prepared cells from glass plates with non-transparent gold electrodes prepared by evaporation. Due to the high conductivity of the electrodes the high frequency mode, that is present in the frequency range of about 1 MHz if ITO electrodes are used, was shifted to higher frequency by one order of magnitude. With cells with gold electrodes weak high frequency modes could be studied. Dielectric properties were studied using a Schlumberger 1260 impedance analyzer. The frequency dispersions were measured on cooling at a rate of about  $0.2 \text{ K min}^{-1}$ , keeping the temperature of the sample stable during frequency sweeps in the range of 10 Hz–1 MHz. The frequency dispersion data were analyzed using the Cole–Cole formula for the frequency dependent complex permittivity

$$\varepsilon^*(f) = \varepsilon' - i\varepsilon''$$

$$\varepsilon^* - \varepsilon_\infty = \frac{\Delta\varepsilon}{1 + (if/f_r)^{(1-\alpha)}} - i \frac{\sigma}{2\pi\varepsilon_0 f^n} + Af^m \quad (1)$$

where  $f_r$  is the relaxation frequency,  $\Delta\varepsilon$  is dielectric strength,  $\alpha$  is the distribution parameter of the relaxation,  $\varepsilon_0$  is the permittivity of a vacuum,  $\varepsilon_\infty$  is the high frequency permittivity and  $m$ ,  $A$  are fitting parameters. The second and third terms in the equation are used to eliminate a low frequency contribution from the dc conductivity  $\sigma$  and a high frequency contribution due to the resistance of the ITO electrodes, respectively.

SHG measurements were performed using a Q-switched Nd–YAG laser (6 ns pulses at 20 Hz,  $\lambda = 1064$  nm). The sample was turned 45 degrees with respect to the beam direction and the fundamental wave had p-polarization. The SH signal at 532 nm was detected by a photomultiplier and boxcar averager. To avoid sample damage very weak pulses ( $<0.1$  mJ) were used, without any focusing. The spot size 1 mm allowed investigation of the average signal from the observed texture. SHG hysteresis loops were measured using a very low frequency (0.01–0.003 Hz) triangular voltage.

X-Ray studies were performed using a DRON system equipped with a graphite monochromator. Experiments were conducted on non-oriented samples in the reflection mode.

## Results

The phase transition temperatures and enthalpies were determined from DSC studies. Typical DSC plots are presented in Fig. 1a, b, and c for the second heating and cooling runs for substances **4a**, **4b** and **4c**, respectively. The phase transition from the isotropic to the high temperature mesophase is accompanied by a high transition enthalpy. This phase was identified as the  $B_2$  phase from texture observation in a polarising microscope and characterized under an applied electric field. Another phase transition was detected on cooling (see Fig. 1). X-Ray studies indicated that this phase had crystalline character and we denoted it as CrX (see below). This assumption is supported by relatively broad overcooling

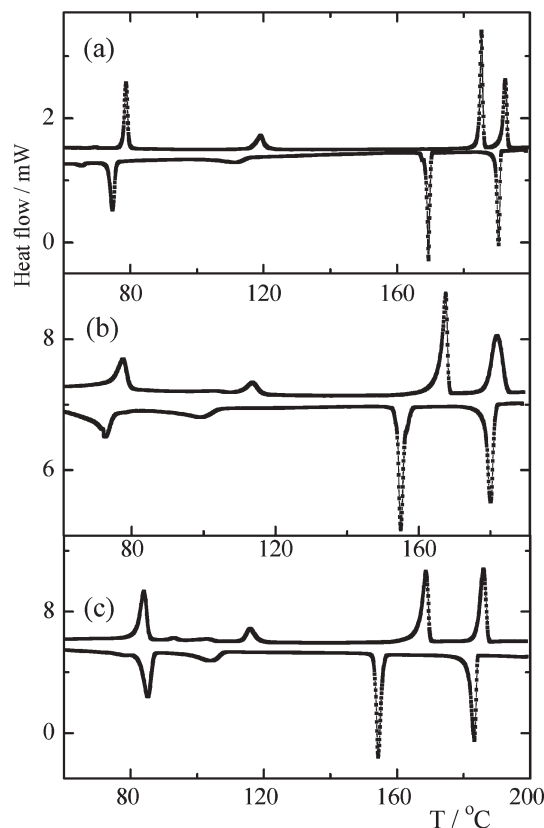


**Fig. 1** DSC plots for compounds (a) **4a**, (b) **4b** and (c) **4c**. The upper and lower curves show the second heating and cooling runs, respectively. The slopes are adjusted for convenience.

of the  $B_2$  phase (see the melting point in Table 1). The transition temperatures and associated enthalpy changes are summarised in Table 1. Other peaks seen at low temperatures (Fig. 1) represent the phase transitions in the solid state.

The high temperature phase observed for all materials exhibits a fan-shaped texture, typical for the  $B_2$  phase. On fast cooling from the isotropic phase the fans appear with stripes parallel to the smectic layers. Under a dc electric field of  $0.5\text{--}1 \text{ V } \mu\text{m}^{-1}$  the stripes disappear.

On very slow cooling from the isotropic phase (rates lower than  $0.1 \text{ K min}^{-1}$ ) two types of domain could be obtained instead of narrow stripes (see Fig. 2a for **4f**). Using monochromatic light we could distinguish different behaviour of domains when decrossing the analyzer. One type of domain (green domains in Fig. 2a) exhibits optical extinction in crossed polarizers along the smectic layer normal. The other type of domain (yellow domains in Fig. 2a) exhibits extinction at decrossed polarizers, which indicates the rotation of the polarized light plane. On the basis of this fact, we consider that the director is twisted within the smectic layers along the sample plane normal and call these domains *twisted*. The birefringence,  $\Delta n$ , measured by a calibrated Babinet–Soleil compensator, has been evaluated for the first type of domain, which has ordinary optical properties, *i.e.* four extinction brushes for crossed polarizer and analyzer. Compensation was obtained in the second and third order of interference light spectra and the birefringence reaches relatively high values

**Table 1** Melting point, mp, indicated on second heating, phase transition temperatures,  $T_{tr}$ , and corresponding enthalpies,  $\Delta H$ , detected on second cooling are in square brackets. All thermograms were taken at a rate of 5 K  $\text{min}^{-1}$ .  $R_1$ ,  $R_2$  are alkyl or alkoxy chains corresponding to Scheme 1

	$R_1$	$R_2$	mp/ $^{\circ}\text{C}$ [ $\Delta H/\text{J g}^{-1}$ ]	$T_{tr}/^{\circ}\text{C}$ [ $\Delta H/\text{J g}^{-1}$ ]	CrX	$T/^{\circ}\text{C}$ [ $\Delta H/\text{J g}^{-1}$ ]	$B_2$	$T/^{\circ}\text{C}$ [ $\Delta H/\text{J g}^{-1}$ ]	Iso
<b>4a</b>	–OC <sub>8</sub> H <sub>17</sub>	–OC <sub>8</sub> H <sub>17</sub>	185 [+34.7]	76 [–21.1]	•	170 [–35.5]	•	191 [–30.9]	•
<b>4b</b>	–OC <sub>11</sub> H <sub>23</sub>	–OC <sub>11</sub> H <sub>23</sub>	168 [+28.8]	94 [–32.2]	•	159 [–34.4]	•	189 [–28.4]	•
<b>4c</b>	–OC <sub>11</sub> H <sub>23</sub>	–C <sub>11</sub> H <sub>23</sub>	171 [+24.5]	62 [–24.7]	•	146 [–23.6]	•	179 [–24.3]	•
<b>4d</b>	–C <sub>11</sub> H <sub>23</sub>	–OC <sub>11</sub> H <sub>23</sub>	172 [+25.3]	114 [–4.7]	•	164 [–24.7]	•	185 [–23.4]	•
<b>4e</b>	–C <sub>10</sub> H <sub>21</sub>	–C <sub>10</sub> H <sub>21</sub>	171 [+25.1]	66 [–8.1]	•	155 [–8.0]	•	171 [–25.2]	•
<b>4f</b>	–OC <sub>9</sub> H <sub>18</sub> CH=CH <sub>2</sub>	–OC <sub>11</sub> H <sub>23</sub>	168 [+26.6]	91 [–5.2]	•	157 [–25.1]	•	182 [–23.1]	•
<b>4g</b>	–C <sub>8</sub> H <sub>17</sub>	–OC <sub>9</sub> H <sub>18</sub> CH=CH <sub>2</sub>	173 [+29.5]	95 [–4.2]	•	162 [–27.7]	•	183 [–25.6]	•
<b>4h</b>	–OC <sub>10</sub> H <sub>21</sub>	–OC <sub>9</sub> H <sub>18</sub> CH=CH <sub>2</sub>	166 [+24.7]	73 [–18.9]	•	156 [–25.9]	•	181 [–25.0]	•
<b>4i</b>	–OC <sub>11</sub> H <sub>23</sub>	–OC <sub>9</sub> H <sub>18</sub> CH=CH <sub>2</sub>	167 [+27.7]	86 [–18.9]	•	156 [–25.7]	•	184 [–25.3]	•

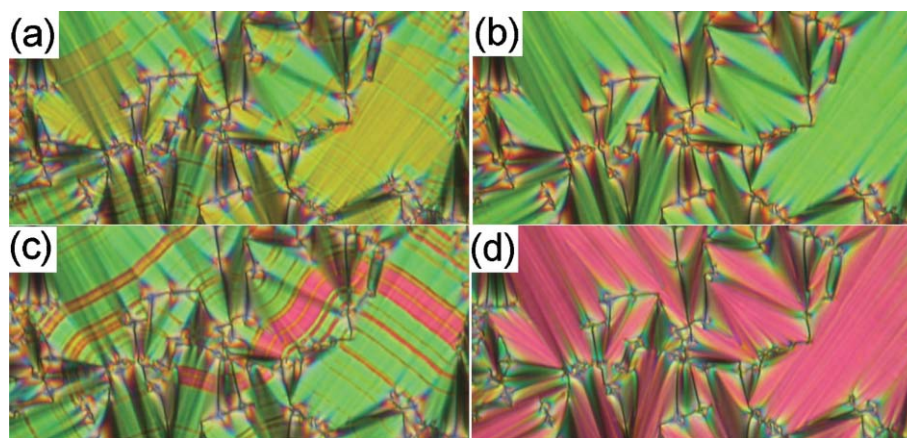


**Fig. 2** Planar texture of compound **4f** in the  $B_2$  phase at  $T = 170$   $^{\circ}\text{C}$ . (a) Domains obtained on slow cooling from the isotropic phase. The yellow domains (twisted) rotate the polarized light plane. Also shown is the same part of the sample under a dc electric field of (b) 1  $\text{V } \mu\text{m}^{-1}$ , (c) 10  $\text{V } \mu\text{m}^{-1}$ , (d) 15  $\text{V } \mu\text{m}^{-1}$ . The width of the figures corresponds to 200  $\mu\text{m}$ .

within 0.20 and 0.28 for the studied materials (0.26 for green domains of **4f**, see Fig. 2a). Applying a dc electric field of about 0.5  $\text{V } \mu\text{m}^{-1}$  (threshold field  $E_1$ ) causes the twisted domains to gradually disappear and the sample becomes almost homogeneously coloured (green fans in Fig. 2b). By increasing the value of the applied dc field to the threshold field  $E_2$  (1–10  $\text{V } \mu\text{m}^{-1}$ , varying for studied compounds) we induce a phase transition accompanied by a birefringence change. The transition is seen in Fig. 2c, where the red domains correspond to the high field structure. The saturated field state texture with homogeneously coloured fans is shown in Fig. 2d. The birefringence of domains in an electric field is even higher than that without a field (0.32 for red domains of **4f**, see Fig. 2d). After switching off the dc field the twisted domains usually reappear in the form of narrow stripes so that the texture resembles the virgin texture reached on fast cooling. The extinction position parallel to the layer normal remains up to the maximum of applied voltage 40  $\text{V } \mu\text{m}^{-1}$ , when a short cut usually takes place.

For compounds **4c**, **4d** and **4g** even under lower dc field (0.2–0.5  $\text{V } \mu\text{m}^{-1}$ ) a direct phase transition to the ferroelectric phase takes place, without forming the transient homogeneous texture as described in the previous case and shown in Fig. 2b. Such compounds exhibit only one peak in the polarization current profile (see the next paragraph).

On further cooling the phase transition from the  $B_2$  phase to the low temperature phase takes place. The birefringence of

fans slightly changes in the planar texture, and cracks and additional defects appear. The low temperature phase does not switch in the applied electric field. The  $B_2$  and the low temperature CrX phases, which are hardly recognizable in the planar texture without an applied field could be recognized under an applied dc voltage because of the different birefringence colors. The coexistence of both phases (Fig. 3) was observed within a temperature interval of several degrees.

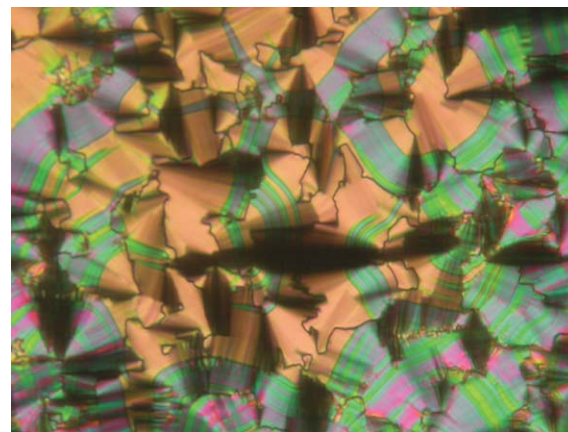


**Fig. 3** Fan-shaped texture at the  $B_2$ –CrX phase transition under a dc electric field for **4b** in the planar cell. Orange fans represent the  $B_2$  phase. The width of the figure corresponds to 300  $\mu\text{m}$ .

Free standing films (FSF) have been successfully prepared and studied for all compounds. The phase transition from the isotropic to the  $B_2$  phase in FSF is accompanied with the formation of bubbles and defects (see Fig. 4a). The typical schlieren texture of the  $B_2$  phase transforms into a crystalline-like texture (Fig. 4). On further cooling the FSF usually breaks through.

Switching was studied under a triangular wave field of  $25 \text{ V}_{\text{pp}} \mu\text{m}^{-1}$ , 8–11 Hz. Two different types of polarization current profile were observed. Most of the compounds exhibit two distinct peaks per half period in the polarization current in the  $B_2$  phase. For three compounds mentioned previously (**4c**, **4d** and **4g**) only one sharp peak was found. In Fig. 5a–d, we can compare the polarization current profiles for compounds **4b**, **4c**, **4d** and **4f**, respectively.

SHG measurements were performed in the  $B_2$  phase at temperatures of about 10 K below the isotropic– $B_2$  phase transition in a quasi-static electric field. For all studied compounds zero SHG signal was detected up to the electric field corresponding to the threshold value  $E_2$ . A steep increase of SHG signal with increasing field occurred for electric field  $E > E_2$ . For compounds **4b** and **4f**, which may exhibit twisted domains under very slow cooling and subsequent two stage switching and also single peak switching current in an ac field,  $E_2$  is relatively high (see Fig. 6a), as is typical for antiferroelectric banana liquid crystals.<sup>9,8,18</sup> For compounds **4c**, **4d** and **4g** the steep increase of the SHG signal occurs at an electric field one order of magnitude smaller (see Fig. 6b), indicating ferroelectric behavior. This is consistent with the low threshold

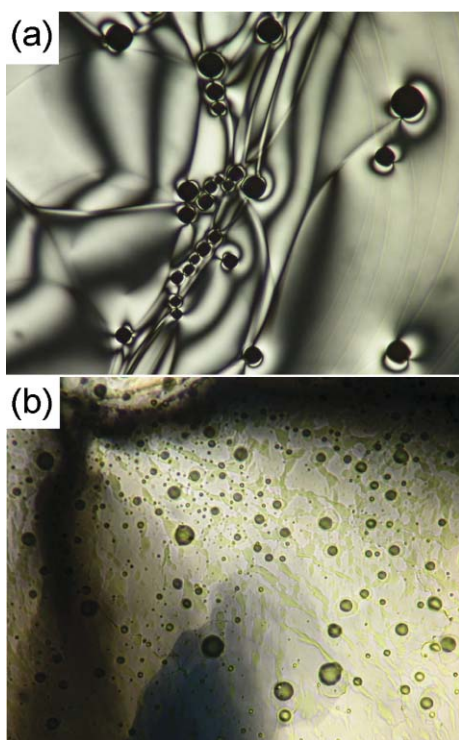


**Fig. 4** Texture of free-standing film of compound **4b** (a) in the  $B_2$  phase below the phase transition from the isotropic phase, at a temperature of  $T = 188 \text{ }^\circ\text{C}$ , (b) in the CrX phase, at about  $T = 148 \text{ }^\circ\text{C}$ . The width of the figures corresponds to about  $200 \mu\text{m}$ .

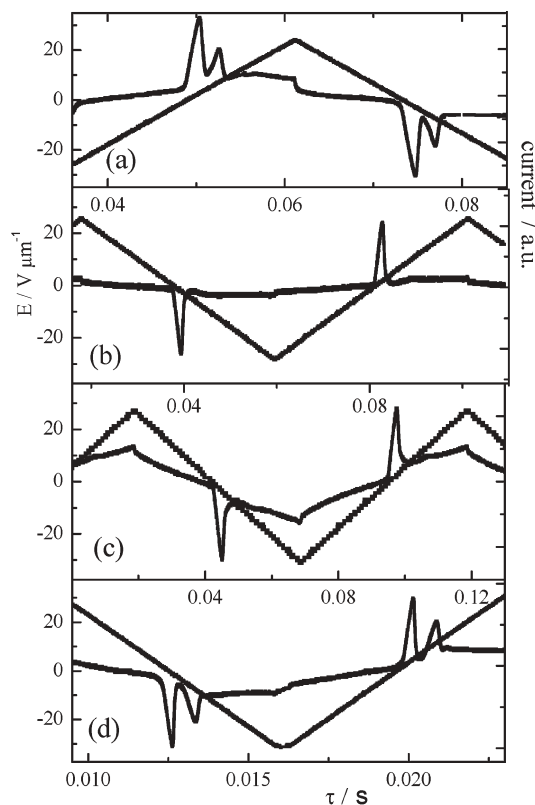


**Fig. 5** Switching current profile for compounds (a) **4b**, (b) **4c**, (c) **4d** and (d) **4f** in the  $B_2$  phase at a temperature of 10 degrees below the phase transition from the isotropic phase, at a frequency of 8–11 Hz.

field for transformation into the ferroelectric state detected in the texture observation.

In the dielectric spectroscopy measurements, a weak single relaxation process in the range of hundreds of kHz appeared in the  $B_2$  phase for all studied compounds. Three-dimensional plots of the imaginary part of the dielectric permittivity *versus* temperature are presented in Fig. 7. By fitting the data to eqn (1) we obtained the temperature dependences of the dielectric strength,  $\Delta\epsilon(T)$ , and relaxation frequency,  $f_r(T)$ . Due to the high contribution to the low frequency conductivity we cannot analyze the dielectric spectroscopy data at frequencies below 1 kHz. Two typical temperature dependences are shown in Fig. 8a, b. On cooling from isotropic phase  $\Delta\epsilon$  steeply increases at the isotropic– $B_2$  phase transition and within the  $B_2$  phase only decreases slightly when the temperature decreases. The mode is exponentially quenched in the CrX phase. The low values of  $\Delta\epsilon$  and high relaxation frequency  $f_r$  (100–600 kHz) indicate the antiferroelectric character of the  $B_2$  phase.

In the  $B_2$  phase, application of a bias electric field leads firstly to the increase of  $\Delta\epsilon$  and decrease of  $f_r$  (see Fig. 9) and the mode is suppressed at the value of threshold field  $E_2$ , when the phase transition to the ferroelectric phase takes place. In planar textures it corresponds to a step change of birefringence in the electric field  $E > E_2$  (see Fig. 2c and d).

The X-ray pattern exhibits sharp small angle reflections and a diffuse scattering maximum in the large angle region. This indicates a layered structure with liquid-like molecular packing within the layers. From the inner reflections the layer spacing,

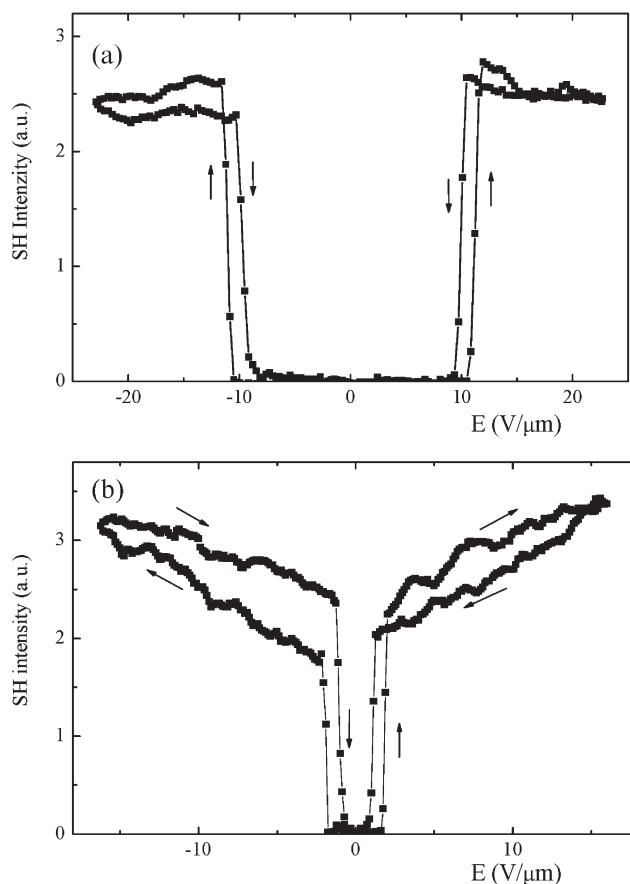


**Fig. 6** SHG signal versus dc electric field for compounds (a) **4b** and (b) **4d**.

$d$ , is determined. The  $d$  values of 49.6 Å for **4b**, 50.4 Å for **4f** and 50.8 Å for **4i** were determined at the temperature 15 degrees below the isotropic- $B_2$  phase transition. For all studied compounds we found the layer spacing to be smaller than their calculated molecular length,  $l$ , which points to a tilted arrangement of molecules.

On cooling there is a strong first order transition to the CrX phase (jump in  $d$  and coexistence of two signals). The X-ray patterns indicate a high degree of ordering. So we conclude the CrX phase is probably a crystalline smectic phase. On cooling to still lower temperatures another anomaly is seen on layer spacing and on intensity. The phase below CrX, which is observed also on DSC plots (see Fig. 1), exhibits higher order typical for the solid state.

## Discussion and conclusions

We synthesized thermally stable asymmetrical bent-core mesogens. On cooling from the isotropic phase the  $B_2$  phase appears in all studied compounds. The texture observations in both planar samples and free-standing films are compatible with the  $B_2$  phase structure. The planar samples revealed a typical striped texture. On very slow cooling two types of domain appear instead of stripes. One type rotates the plane of polarized light, indicating a non-homogeneous (twisted) in-plane structure, which is assumed to be imposed by surfaces.

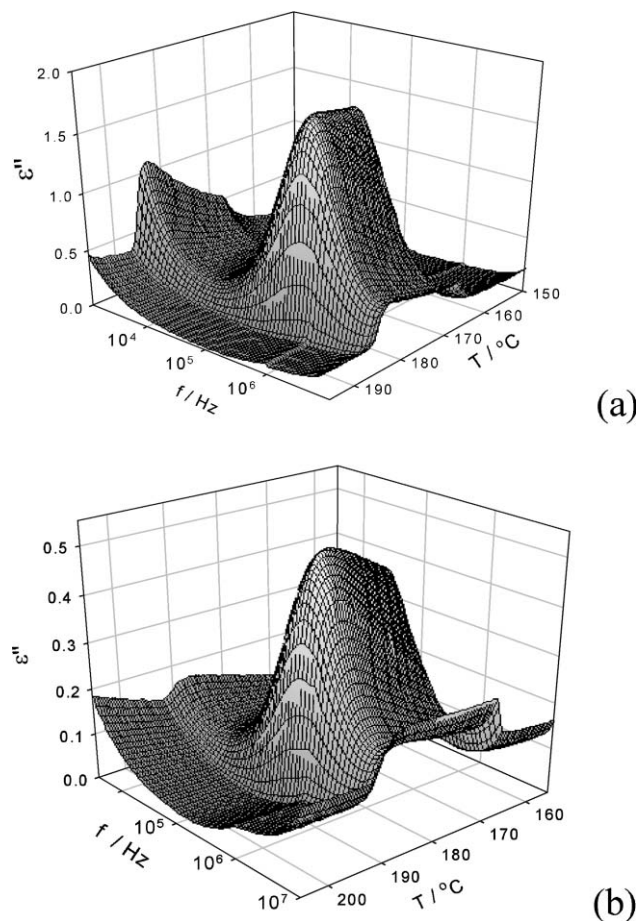


**Fig. 7** Temperature-frequency plots of the imaginary part of the dielectric permittivity taken on cooling from the isotropic phase for compounds (a) **4c** and (b) **4f**.

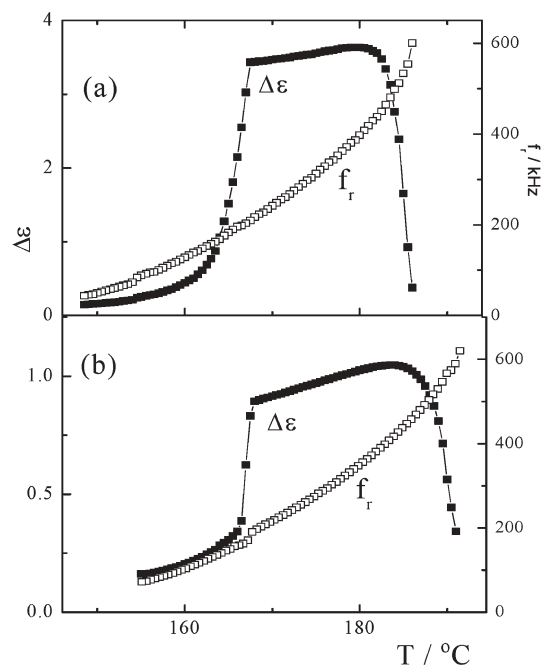


**Fig. 8** Temperature dependences of relaxation frequency,  $f_r$ , and dielectric strength,  $\Delta\epsilon$ , for compounds (a) **4c** and (b) **4f**.

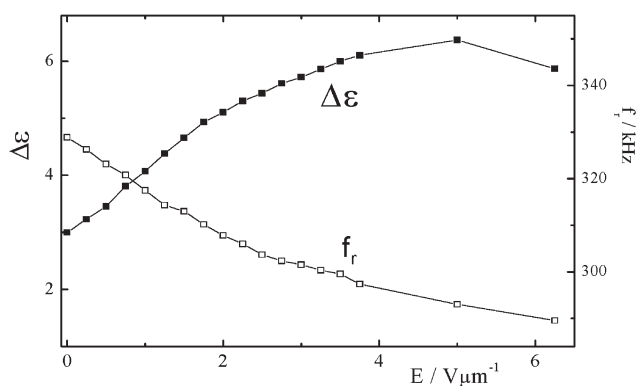


**Fig. 9** Dielectric strength,  $\Delta\epsilon$ , and relaxation frequency,  $f_r$ , plotted as a function of an applied dc bias field in the  $B_2$  phase at the temperature  $T = 176\text{ }^\circ\text{C}$  for compound **4d**.

The domains rotating the plane of polarized light disappear under an electric threshold field,  $E_1$ . For higher electric field  $E_2 > E_1$  switching to the ferroelectric structure takes place. The texture of non-twisted domains exhibits optical extinction in the position when the layer normal is parallel to the crossed polarizers for both zero and high field states, which implies anticlinic structures for both states, and thus the transition between chiral ( $\text{SmC}_A\text{P}_A$ ) and racemic ( $\text{SmC}_A\text{P}_F$ ) phases under the field, when considering the simple model from ref. 2. This model involves the same birefringence in both field-on and field-off structures in contrast to the experimental results, and a change of chirality at the transition. Moreover, the change of chirality can be hardly expected especially for compounds **4c**, **4d** and **4g**, exhibiting extremely low coercive fields. For these reason another model was proposed in refs. 22 and 23, supposing that the structure is composed of mesoscopic chiral domains  $\text{SmC}_A\text{P}_A$  of opposite handedness, which are transformed under the field to the  $\text{SmC}_S\text{P}_F$  structure with the opposite tilt in each domain. Then also the overall structure under the field has the same point symmetry as the anticlinic one, which is in accordance with our observation of switching without change of extinction position parallel to the polarizers. The change of birefringence under the field is expected because of different averaging of optical polarizability on the scale of two layers and/or on the scale of mesoscopic domains.

The behaviour of the twisted domains under the electric field could be described in the schematic model presented in Fig. 10. It is supposed that the equilibrium  $\text{SmC}_A\text{P}_A$  structure occurs only in the sample bulk, but at the surfaces it is modified to the synclinic ferroelectric  $\text{SmC}_S\text{P}_F$  structure due to strong polar surface anchoring. This anchoring also ensures that the preferred molecular polarisations at upper and lower surfaces are opposite. Surface  $\text{SmC}_S\text{P}_F$  and bulk  $\text{SmC}_A\text{P}_A$  structures are mediated by a twist of molecules in the smectic layers along the sample plane normal. The twist is realized by a rotation of bent-shaped molecules along the surface of a cone with polarisations tangential to the cone surfaces (Fig. 10a). When the applied dc electric field reaches the first critical threshold field  $E_1$ , which compensates the polarity of one surface, the  $\text{SmC}_A\text{P}_A$  structure is restored at this surface (Fig. 10b). A further increase of the field leads to unwinding of the twisted

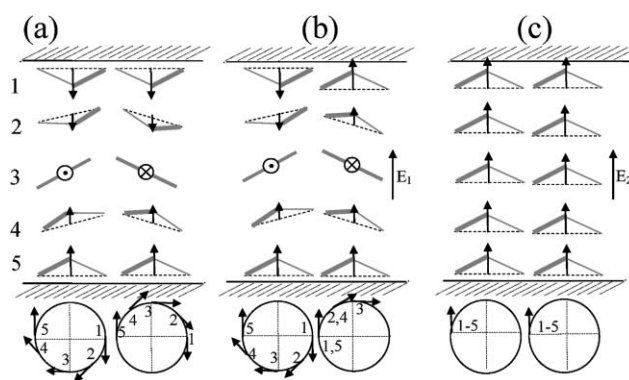


**Fig. 10** Model of switching of the twisted domains in the electric field. (a) Twisted structure without field in the sample cross-section. The glasses are depicted by shading. Bent-shaped molecules rotating on the surface of the cone are represented by triangles where thicker lines show molecular arms inclined toward the observer. Dashed lines indicate the director projected onto the plane of the figure. The arrows show the molecular spontaneous polarizations the length of which corresponds to the projection of polarization onto the plane of the figure. The bottom part illustrates the orientation of polarizations from a side view. Numbers 1–5 correspond to the same molecular positions in the upper part of the figure. (b) Under dc field  $E > E_1$  the antiferroelectric structure is restored at the upper surface resulting in partial unwinding of the twisted structure in every second layer. (c) Complete switching at  $E > E_2$  leading to uniform structures in both layers.

structure and the uniform ferroelectric structure is realized at the threshold field  $E_2$  (Fig. 10b). The detail description of the twisted structure and its behaviour in the electric field is under study.

X-Ray studies confirmed the layer structure and provided the information about the layer spacing in the  $B_2$  phase. The measured values of layer spacing of the studied compounds, 49.6 Å for **4b**, 50.4 Å for **4f** and 50.9 Å for **4i**, are very similar compared to those of compounds with a symmetrical 7-ring core (see ref. 19, where a value of 50.5 Å was presented for a compound which differs from **4i** only in the number of phenyl rings in the core and has the same ending chains). This indicates effective packing of the studied molecules in a way depicted schematically in Fig. 11.

In the studied series we observed two different types of switching properties. Either one or two distinct peaks were

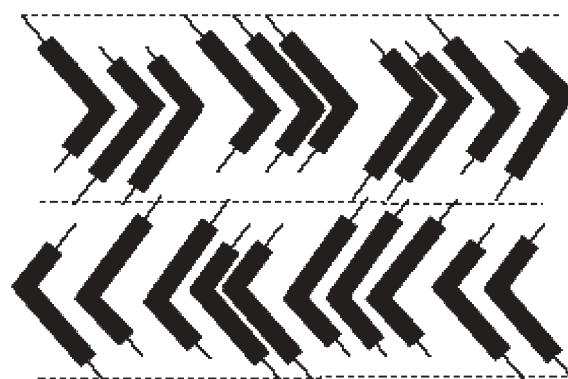


**Fig. 11** Scheme of the molecular packing in layers.

observed in the polarization current profiles (Fig. 5). For compounds **4c**, **4d** and **4g** with only one sharp peak, SHG study shows that all compounds have no SHG signal without electric field (Fig. 6). This indicates a centrosymmetrical ground state. Nevertheless, for compounds **4c**, **4d** and **4g** SHG measurements reveal extremely low field at which the signal starts to grow. Macroscopic polarization at zero field can be cancelled not only in the antiferroelectric structure, but also in the ferroelectric one due to domains or polar surface interactions, which is consistent with our model. In such a case a lower threshold field to reach the saturated ferroelectric state can be expected. From the switching and SHG experiments one cannot conclude if the ground state in **4c**, **4d** and **4g** compounds is ferroelectric or antiferroelectric with a low energetic barrier for transition to the ferroelectric state.

For all studied materials dielectric dispersion data exhibit a weak mode in the frequency range of 100–600 kHz. Such a mode is typical for the antiferroelectric B<sub>2</sub> phase. An anomalous increase of the dielectric strength of this mode with an applied bias lower than the critical threshold value  $E_2$  is in agreement with theoretical predictions for the antiphase phason behaviour<sup>24</sup> in an electric field. We cannot exclude the existence of a relaxation below 1 kHz, which cannot be detected due to the high conductivity of the studied materials and which would be consistent with the ferroelectric phase. But still the detected high frequency relaxation and its behaviour in the bias field can hardly occur in the ferroelectric phase.

The different behaviour of studied ferroelectric-like and typical antiferroelectric compounds is difficult to explain on the basis of their molecular structure. We would like to point out that the common feature of the structures of these three compounds is the dissimilar linkage connecting the aliphatic chains on the short and long molecular arms.

## Acknowledgements

This work was supported by Research Plan AV0Z10100520 and grant No. 202/05/0431 from the Grant Agency of the Czech Republic and KBN grant No. 4T09A 00425.

## References

- 1 T. Niori, T. Sekine, J. Watanabe, T. Furukawa and H. Takezoe, *J. Mater. Chem.*, 1996, **6**, 1231.
- 2 D. R. Link, G. Natale, R. Shao, J. E. MacLennan, N. A. Clark, E. Körblová and D. M. Walba, *Science*, 1997, **278**, 1924.
- 3 D. M. Walba, E. Körblová, R. Shao, J. E. MacLennan, D. R. Link, M. A. Glaser and N. A. Clark, *Science*, 2000, **288**, 2181.
- 4 M. Zennyoji, Y. Takanishi, K. Ishikawa, J. Thisayukta, J. Watanabe and H. Takezoe, *J. Mater. Chem.*, 1999, **9**, 2775.
- 5 H. Nádasi, W. Weissflog, A. Eremin, G. Pelzl, S. Diele, B. Das and S. Grande, *J. Mater. Chem.*, 2002, **12**, 1316.
- 6 M. Nakata, D. R. Link, F. Thisayukta, Y. Takanishi, K. Ishikawa, J. Watanabe and H. Takezoe, *Liq. Cryst.*, 2001, **28**, 1301.
- 7 M. Kašpar, V. Hamplová, V. Novotná, M. Glogarová and P. Vaněk, *J. Mater. Chem.*, 2002, **12**, 2221.
- 8 W. Weissflog, G. Naumann, B. Kosata, M. W. Schröder, A. Eremin, S. Diele, Z. Vakhovskaya, H. Kresse, R. Friedemann, S. Ananda, R. Krishnan and G. Pelzl, *J. Mater. Chem.*, 2005, **15**, 4328.
- 9 K. Kumazawa, M. Nakata, F. Araoka, Y. Takanishi, K. Ishikawa, J. Watanabe and H. Takezoe, *J. Mater. Chem.*, 2004, **14**, 157.
- 10 E. Gorecka, D. Pocięcha, F. Araoka, J. Thisayukta, Y. Takanishi, K. Ishikawa, J. Watanabe and H. Takezoe, *Phys. Rev. E*, 2000, **62**, R4524.
- 11 V. Novotná, V. Hamplová, M. Kašpar, M. Glogarová, K. Knížek, S. Diele, G. Pelzl, Ch. Jones, D. Coleman and N. A. Clark, *Liq. Cryst.*, 2005, **32**, 967.
- 12 R. Amaranatha Reddy and B. K. Sadashiva, *Liq. Cryst.*, 2003, **30**, 1031.
- 13 J. Mieczkowski, K. Gomola, J. Koseska, D. Pocięcha, J. Szydłowska and E. Gorecka, *J. Mater. Chem.*, 2003, **13**, 2132.
- 14 R. Amaranatha Reddy and B. K. Sadashiva, *Liq. Cryst.*, 2004, **31**, 1069.
- 15 U. Dunemann, M. W. Schröder, G. Pelzl, S. Diele and W. Weissflog, *Liq. Cryst.*, 2005, **32**, 151.
- 16 V. Prasad and A. Jakli, *Liq. Cryst.*, 2004, **31**, 473.
- 17 R. Achten, R. Cuypers, M. Giesbergs, A. Koudijs, A. T. M. Marcelis and E. J. R. Sudhölter, *Liq. Cryst.*, 2004, **31**, 1167.
- 18 H. N. Shreenivasa and B. K. Sadashiva, *J. Mater. Chem.*, 2004, **14**, 2813.
- 19 R. A. Reddy and C. Tschierske, *J. Mater. Chem.*, 2006, **16**, 907.
- 20 V. Novotná, V. Hamplová, M. Kašpar, M. Glogarová and D. Pocięcha, *Liq. Cryst.*, 2005, **32**, 1115.
- 21 M. Kašpar, M. Glogarová, V. Hamplová, H. Sverenyák and S. A. Pachomov, *Ferroelectrics*, 1993, **148**, 103.
- 22 C. L. Folcia, J. Ortega and J. Etxebarria, *Liq. Cryst.*, 2003, **30**, 1189.
- 23 P. Pyc, J. Mieczkowski, D. Pocięcha, E. Gorecka, B. Donnio and D. Guillon, *J. Mater. Chem.*, 2004, **14**, 2374.
- 24 D. Pocięcha, E. Gorecka, M. Čepič, N. Vaupotič, K. Gomola and J. Mieczkowski, *Phys. Rev. E*, 2005, **72**, 060701R.